

Knockdown of occludin expression leads to diverse phenotypic alterations in epithelial cells

Alan S. L. Yu,² Karin M. McCarthy,¹ Stacy A. Francis,¹ Joanne M. McCormack,¹ Jean Lai,⁴ Rick A. Rogers,⁴ Robert D. Lynch,³ and Eveline E. Schneeberger¹

¹Molecular Pathology Unit, Massachusetts General Hospital, Charlestown, Massachusetts; ²Department of Medicine and Department of Physiology and Biophysics, University of Southern California Keck School of Medicine, Los Angeles, California; ³Department of Biological Sciences, University of Massachusetts at Lowell, Lowell, Massachusetts; and ⁴Physiology Program, Harvard School of Public Health, Boston, Massachusetts

Submitted 29 November 2004; accepted in final form 31 January 2005

Yu, Alan S. L., Karin M. McCarthy, Stacy A. Francis, Joanne M. McCormack, Jean Lai, Rick A. Rogers, Robert D. Lynch, and Eveline E. Schneeberger. Knockdown of occludin expression leads to diverse phenotypic alterations in epithelial cells. *Am J Physiol Cell Physiol* 288: C1231–C1241, 2005. First published February 2, 2005; doi:10.1152/ajpcell.00581.2004.—The function of occludin (Occ) in the tight junction is undefined. To gain insight into its role in epithelial cell biology, occludin levels in Madin-Darby canine kidney II cells were suppressed by stably expressing short interfering RNA. Suppression of occludin was associated with a decrease in claudins-1 and -7 and an increase in claudins-3 and -4. Claudin-2 levels were unaffected. The tight junction “fence” function was not impaired in suppressed Occ (Occ⁻) clones, as determined by BODIPY-sphingomyelin diffusion in the membrane. The most striking changes were those related to control of the cytoskeleton and the “gate” function of tight junctions. A reduced ability of Occ⁻ clones to extrude apoptotic cells from the monolayers suggested that neighbors of apoptotic cells either failed to sense their presence or were unable to coordinate cytoskeletal activity necessary for their extrusion. To further test the extent to which actin cytoskeletal activity depends on the presence of occludin, Occ⁻ and Occ⁺ monolayers were depleted of cholesterol. Previous studies showed that cholesterol depletion is associated with reorganization of the actin cytoskeleton and a fall in transepithelial electrical resistance. In contrast to control Occ (Occ⁺) cells, transepithelial electrical resistance did not fall significantly in cholesterol-depleted Occ⁻ monolayers and they failed to generate Rho-GTP, one of the signaling molecules involved in regulating the actin cytoskeleton. While steady-state transepithelial electrical resistance was similar in all clones, tight junction permeability to mono- and divalent inorganic cations was increased in Occ⁻ monolayers. In addition, there was a disproportionately large increase in permeability to monovalent organic cations, up to 6.96 Å in diameter. Chloride permeability was unaffected and there was little change in mannitol flux. The data suggest that occludin transduces external (apoptotic cells) and intramembrane (rapid cholesterol depletion) signals via a Rho signaling pathway that, in turn, elicits reorganization of the actin cytoskeleton. Impaired signaling in the absence of occludin may also alter the dynamic behavior of tight junction strands, as reflected by an increase in permeability to large organic cations; the permeability of ion pores formed of claudins, however, is less affected.

tight junction; occludin; Rho-GTP

THE TIGHT JUNCTION (TJ) is a continuous, circumferential beltlike structure that forms a permeability barrier at the apical end of the intercellular space (11), where it regulates the passage of

water, ions, and small noncharged solutes through the paracellular pathway (24, 41, 45). Occludin, the first integral TJ protein to be identified (15), is an ~60-kDa tetraspan membrane protein that forms two extracellular loops flanked by cytoplasmic amino and COOH termini. The two extracellular domains are unusually rich in tyrosine and glycine residues, and they contain relatively few charged residues. Although clearly localized at the TJ, the question remained whether occludin alone could account for the permeability properties of TJs (30). Evidence for the presence of additional, integral TJ proteins was obtained when embryonic stem cells, in which both occludin alleles had been disrupted by homologous recombination, were found to express functionally competent TJs and displayed normal appearing TJ strands in freeze-fracture replicas (37). These observations led to a renewed search for additional integral TJ proteins, which resulted in the discovery of the claudins, a now 24-member family of proteins (13, 45). Claudins, like occludin, are tetraspan proteins, but they differ from occludin in a number of significant ways. Their molecular mass ranges from 20 to 27 kDa, and their extracellular loops contain variously charged amino acid residues that together produce isoelectric points in the two extracellular domains ranging from 4.05 to 10.50 (27). The role of claudins in regulating the specific ion permeability of the paracellular pathway is currently an area of active investigation (8, 9, 42, 46, 47).

The function of occludin, however, remains undefined. Studies in which either full-length or COOH-terminally truncated occludin was overexpressed in epithelial cells resulted in not only an elevated transepithelial electrical resistance (TER) but also an unexpected increase in mannitol flux (2, 26). Conversely, when epithelial cells were transfected with oncogenic Raf-1, expression of both occludin and claudin-1 was down-regulated and functional TJs were lost. Interestingly, introduction of the occludin gene into these transformed cells completely restored the junctional complex (21). More puzzling were the observations made in occludin-null mice (38). Newborn occludin^{-/-} mice survive, but they show considerable retardation in postnatal growth. Occludin^{-/-} male mice are sterile, whereas occludin^{-/-} females produce normal litters when mated with wild-type males; however, they fail to suckle their young. In addition, chronic inflammation and epithelial hyperplasia are observed in the gastric mucosa, as well as a

Address for reprint requests and other correspondence: E. E. Schneeberger, Molecular Pathology Unit, 149-7151, Massachusetts General Hospital East, 149 13th St., Charlestown, MA 02129 (E-mail: eschneeberger@partners.org).

The costs of publication of this article were defrayed in part by the payment of page charges. The article must therefore be hereby marked “advertisement” in accordance with 18 U.S.C. Section 1734 solely to indicate this fact.

loss of cytoplasmic granules in striated duct cells of the salivary gland, brain calcification, testicular atrophy, and loss of compact bone (38).

The study of gene deletion in mice yields valuable insights into the function of a particular gene. However, ablation of a single gene in animals may be associated with an upregulated expression of other gene products, either as a compensatory response or as an indication of a redundancy in function of other molecules of similar function (18). Furthermore, overexpression of truncated or mutated forms of a protein may significantly perturb the organization and function of endogenous TJ proteins, leading to a phenotype that does not necessarily reflect the function of the protein in question. To gain further insight into the role of occludin at the cellular level, we chose to suppress occludin gene expression at the cellular level utilizing the recently described strategy in which the intracellular synthesis of small interfering RNAs (siRNAs) efficiently and specifically downregulate gene expression (6).

MATERIALS AND METHODS

Reagents

Culture media and Lipofectamine were obtained from Invitrogen (Carlsbad, CA). Penicillin and streptomycin (P/S), hygromycin, and serum were from Sigma (St. Louis, MO).

Cells

COS-7 cells (a gift from Dr. I. Stamenkovic) were cultured in Dulbecco's modified Eagle's medium (DMEM), 10% fetal bovine serum (FBS), and 1% P/S. Madin-Darby canine kidney (MDCK) cells (clone 23) (a gift from Dr. W. J. Nelson) were utilized because they are more readily transfected than CCL34 MDCK cells. Cells in which siRNA occludin expression is suppressed are referred to as Occ⁻ cells. Control Occ⁺ cells were transfected with a cDNA construct that did not suppress occludin expression in COS-7 cells. Six clones each of Occ⁻ and Occ⁺ cells were maintained in DMEM, 10% FBS, 1% P/S, and 150 μ g/ml hygromycin. Cells were split weekly at a ratio of 1:6, and medium was changed every 2–3 days.

Stable clones with suppressed occludin expression were generated by a siRNA strategy using the pSuper vector, in which the H1-RNA promoter was cloned in front of the specific target sequence (a gift from Dr. S. Pillai) (6). Five pairs of 64-nucleotide (nt) complementary oligonucleotides containing a unique 19-nt sequence to different regions of dog occludin DNA, as determined by a basic local alignment tool search, were synthesized by MWG (High Point, NC). The five 19-nt sequences start at nt 364, 877, 1,354, 1,480, and 1,556, respectively, of the dog occludin sequence (GenBank accession no. U49221) (Fig. 1A). These were annealed and ligated unidirectionally into *Bgl*III and *Hind*III sites of the pSuper vector, generating the corresponding constructs 1–5. Screening was performed in COS-7 cells by transient cotransfection of the pSuper constructs together with an expression vector for vesicular stomatitis virus G (VSVG)-tagged dog occludin. Three days later, monolayers were processed for SDS-PAGE and immunoblotted with anti-VSVG antibody. Suppression of VSVG-occludin ranged from 0 to 98%. Two constructs (2 and 4) showing the greatest suppression were cotransfected with a hygromycin expression vector, ptK-Hyg (BD Biosciences Clontech, Palo Alto, CA), into MDCK cells using Lipofectamine 2000. Transfected cells were subcloned and screened for occludin by Western blot analysis. Six clones from construct 4 (19-nt sequence unique to occludin: 5'GTG AAG AGT ACA TGG CTG C-3') showing 96 to 98% suppression were selected. Maximum suppression of construct 2 was only 50%. Transfection with construct 1, which did not suppress occludin, produced six control clones that expressed amounts of occludin similar to those of wild-type cultures.

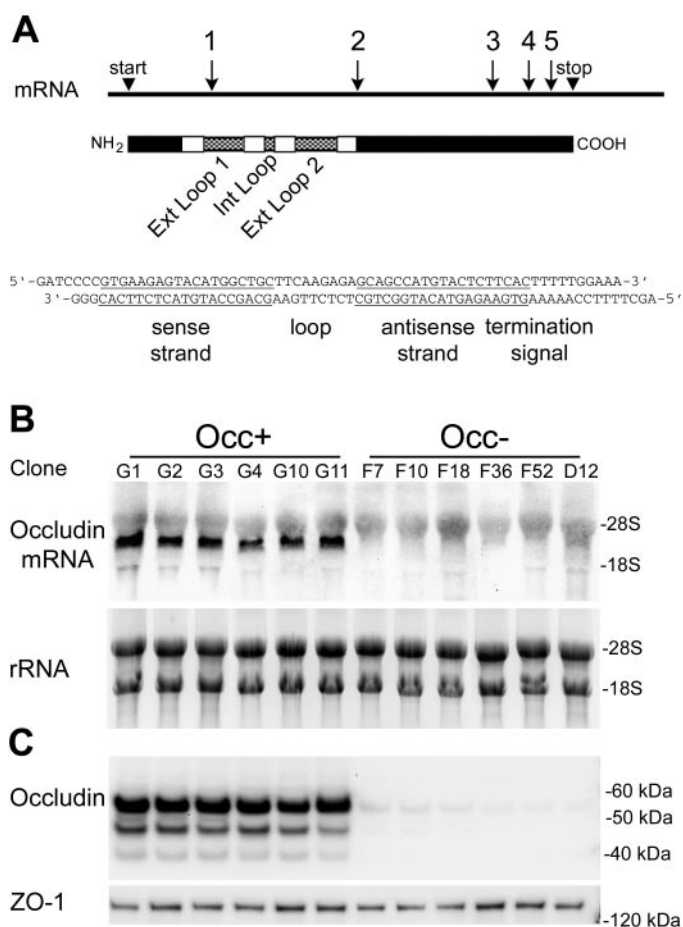


Fig. 1. **A**: small interfering RNA (siRNA) oligonucleotide sites in occludin. Top line represents the 1,563-nt mRNA of occludin (Occ). Vertical arrows indicate approximate sites of the 5 sequences chosen for the siRNA constructs, of which *sequence 1* is the nonsuppressive construct used in the 6 control clones, *sequence 2* suppressed 50%, and *sequence 4* suppressed occludin expression up to 98%. Diagram below represents the intracellular (black), transmembrane (white), the two extracellular (Ext), and single intracellular domains (cross hatched) of occludin protein. Protein and mRNA diagrams are drawn to approximate scale so that relative locations of the siRNA oligonucleotides correspond to segments of the occludin protein below. The 64-nt complementary oligonucleotide pair that yielded maximum occludin suppression is shown. **B**: Northern blot of the 6 control (Occ⁺) and suppressed (Occ⁻) clones. No occludin mRNA was detected in Occ⁻ clones compared with Occ⁺ clones. The 18S and 28S ribosomal RNA bands indicate equal loading. **C**: Western blot probed for occludin showing 96–98% suppression of occludin protein expression in the 6 Occ⁻ compared with the 6 Occ⁺ clones. Zonula occludens-1 (ZO-1) bands indicate equal loading.

TER Measurements

For repeated, sequential TER measurements of individual monolayers on Millicell HA inserts (0.6 cm²) (Millipore, Bedford, MA), a Millicell-ERS epithelial voltohmmeter (World Precision Instruments, New Haven, CT) was utilized at 37°C with electrodes reproducibly placed. TER values ($\Omega \times \text{cm}^2$) were calculated by subtracting the contribution of the bare filter and medium and multiplying by the surface area of the filter.

Calcium Switch Assay

Occ⁻ or Occ⁺ cells were cultured in quadruplicate inserts for 5 days to achieve steady-state TER; medium was changed on alternate days. Monolayers were rinsed three times with Ca²⁺- and Mg²⁺-free

Dulbecco's phosphate-buffered saline (DPBS) and incubated in Ca^{2+} -free, serum-free MEM (SMEM; Invitrogen), 10% dialyzed FBS, 1% P/S, and 150 $\mu\text{g/ml}$ hygromycin for 24 h. The 24-h time interval was chosen to synchronize TJ formation in the various clones. After it was established that TER was at its nadir, the medium was changed to Ca^{2+} -sufficient DMEM and TER was measured at intervals until steady-state values were reached.

Ussing Chamber Electrophysiology Studies

Cells were plated at confluent density on 1-cm² Snapwell polyester filters (Corning Costar) and grown for 6–7 days. Electrophysiological measurements were conducted with the use of an Ussing chamber, with solutions and by methods as previously described (47). Briefly, to determine dilution and bionic potentials, the solution in the basal compartment was changed, whereas that in the apical compartment was maintained in a Ringer solution. For 2:1 NaCl dilution potentials, 150 mM NaCl in Ringer was replaced by 75 mM NaCl and the osmolality was maintained with mannitol. For bionic potentials, 150 mM NaCl was replaced with 150 mM chloride salt of the indicated alkali metal and organic cation. All organic cations used had a $\text{pK}_a > 9.0$ and were therefore completely protonated at pH 7.4. To eliminate traces of Na^+ that could lead to an overestimation of the permeability, multiple washes with Na^+ -free, organic cation-containing buffer were performed.

Paracellular Flux Measurements

[¹⁴C]ethanolamine flux. The net flux of [¹⁴C]ethanolamine across the monolayers cultured on quadruplicate Millicell HA inserts for 6 days was measured by two protocols. In the first, flux from the apical (AP) to the basolateral (BL) compartment was measured under conditions of increased hydrostatic pressure. This was accomplished by adding 0.8 ml of DMEM, 10% FBS, 1.0% P/S, 150 $\mu\text{g/ml}$ hygromycin, and 50 μM ethanolamine to the wells of a 12-well plate after 0.5 ml of the same medium supplemented with 0.55 $\mu\text{Ci/ml}$ of [¹⁴C]ethanolamine was added to the inserts. Under these conditions, the level of the solution in the insert was 3.5 mm above that in the well. At 1, 2, and 3 h, 100- μl samples were removed from the well and 100 μl of medium was replenished. At 1 and 3 h, 10- μl samples of AP medium were taken to determine dilution of the label. In the second protocol, flux was measured on monolayers, cultured as described above, under conditions of equal hydrostatic pressure. To avoid excessive dilution of the diffused radiolabeled tracer, flux was measured in the BL-to-AP direction as follows. The medium was maintained at the same level in the insert and well by the addition of 0.5 and 0.6 ml of DMEM, 10% FBS, 1.0% P/S, 150 $\mu\text{g/ml}$ hygromycin, 50 μM ethanolamine medium to the inserts and wells of a 24-well plate, respectively. In this assay, 0.55 $\mu\text{Ci/ml}$ [¹⁴C]ethanolamine (Amersham Biosciences, Piscataway, NJ) was added to the well and flux was allowed to proceed from the BL to the AP compartment for 1 h, at which time 400 and 10 μl were obtained from the insert and well, respectively. Samples were mixed with Ultima-Gold fluor (Packard Instruments, Meriden, CT) and counted in a Packard 1900TR liquid scintillation counter.

[³H]mannitol flux. [³H]mannitol flux measurements were conducted identically to those described above, except that 1 mM non-radioactive mannitol was added to the medium and 4 $\mu\text{Ci/ml}$ of [³H]mannitol (NEN Life Sciences Products, Boston, MA) was used as tracer. The rate of flux was calculated by regression analysis.

FITC-dextran flux. FITC-dextran flux measurements were conducted on quadruplicate monolayers that had been cultured for 7 days in Millicell inserts by adding 200 μl of 1 mg/ml of either 3- or 10-kDa FITC-dextran (Molecular Probes) in phenol red-free DMEM to the inserts and 600 μl of medium to the well. The monolayers were incubated for 3 h at 37°C. Duplicate 100- μl aliquots were transferred to 96-well plates and measured with the use of a SAFIRE fluorescence plate reader (Tecan Systems, San Jose, CA).

BODIPY-Sphingomyelin Diffusion

Sphingomyelin/BSA complexes (5 μM) were prepared by the addition of BODIPY-C₅-sphingomyelin (Molecular Probes, Eugene, OR) and delipidized BSA (ICN Biomedical, Aurora, OH) to P buffer (10 mM HEPES, pH 7.4, 1 mM sodium pyruvate, 10 mM glucose, 3 mM CaCl_2 and 145 mM NaCl) according to the manufacturer's instructions. Monolayers of Occ+ and Occ- cells were cultured for 5–6 days on tissue culture inserts (A/S Nunc, Roskilde, Denmark). Cells were washed with ice-cold P buffer and labeled by adding 0.5 ml of BODIPY-sphingomyelin/BSA complexes to the insert and 1.0 ml of P buffer to the well. After a 10-min incubation on ice, monolayers were washed in cold P buffer and either directly prepared for confocal microscopy or incubated in P buffer/BSA for 1 h on ice. Filters were removed from the insert and mounted in ice-cold P buffer on a glass slide. Monolayers were examined using a Zeiss LSM 510 laser scanning confocal microscope (Thornwood, NY).

SDS-PAGE and Western Blot Analysis of Whole Cell Preparations

After being washed, the cells were scraped into cold TBS, pelleted by centrifugation, lysed in SDS buffer composed of 5 mM Tris, pH 6.8, 2% SDS, 1 \times Mini EDTA-free protease inhibitor tablet (Roche Diagnostics, Indianapolis, IN), 5 $\mu\text{g/ml}$ DNAase, 10 mM sodium pyrophosphate, 1 mM sodium orthovanadate, and 20 mM sodium fluoride, and stored at -80°C . After being heated in boiling water for 5 min, the samples were sheared six times through a 26-gauge needle. Protein was quantified with the use of a DC protein assay reagent kit (Bio-Rad Laboratories, Hercules, CA). Lysates in SDS sample buffer with 50 mM dithiothreitol were heated at 100°C for 10 min and resolved with the use of NuPage 4–12% Bis-Tris gels (Invitrogen) (20). Proteins were transferred electrophoretically to PVDF membranes (43). After being blocked with TBS-Blotto (10 mM Tris-HCl, pH 7.5, 154 mM NaCl, 5% nonfat dry milk, and 0.05% Tween 20), membranes were incubated with optimal concentrations of primary antibody: hybridoma supernatant R40–76 [rat anti-zonula occludens (ZO-1)] (a gift from D. A. Goodenough), polyclonal rabbit anti-ZO-2, anti-ZO-3, anti-occludin, anti-claudin-1, -2, -3, or -7, anti-junctional adhesion molecule (JAM)-1, mouse monoclonal anti-claudin-4 (all from Zymed), or anti-actin (Sigma) for 1 h at RT. E-cadherin was detected using a 50:50 mixture of RR1 (gift from B. Gumbiner) and 3G8 (gift from W. Gallin) hybridoma supernatants diluted 1:375. Blots were reacted with the appropriate horseradish peroxidase-tagged secondary antibody and detected by enhanced chemiluminescence (PerkinElmer, Boston, MA). MagicMark Western Standard (Invitrogen), which includes recombinant proteins ranging from 20 to 120 kDa, was used to approximate molecular weights. Intensity of protein bands was quantified by densitometry using a Fluor S MultiImager (Bio-Rad).

Differential Detergent Extraction of TJ Proteins

Monolayers of six Occ+ and six Occ- clones were cultured for 6 days as described above. They were rinsed with DPBS to remove floating cells and incubated with Triton X-100 (TX-100) for 30 min at 4°C. The detergent-soluble fraction was harvested and cell debris removed by low-speed centrifugation and an equal volume of 2 \times sample buffer (3% SDS, 0.75 M Tris, pH 8.0, 20% glycerol, and 20 mM DTT). The TX-100 insoluble fraction was scraped into an equal volume of SDS sample buffer. Equal volumes of each fraction were analyzed by SDS-PAGE, and immunoblots prepared for the proteins described above. Densitometry was performed as described above.

Cell adhesion, proliferation, and apoptosis assays. Vybrant cell adhesion assays were conducted using Kit V-13181 (Molecular Probes) according to the manufacturer's instructions. Briefly, cells in suspension were labeled with Calcein AM dye, and equal numbers of cells were plated in 96-well plates. At timed intervals, nonadherent

cells were removed and adherent cells were quantified with the use of a SAFIRE fluorescence plate reader.

Fluorometric DNA determination. DNA was quantified in the six Occ⁻ and six Occ⁺ clones plated in 96-well plates using a fluorometric assay (19). Briefly, after the cells were plated (1×10^5 cells/well/clone) in 96-well plates, medium was aspirated at timed intervals, monolayers were hydrolyzed in 0.5 N perchloric acid for 15 min at 70°C, and 25% diamino benzoic acid dihydrochloride in water was added. After a 2-h incubation period at 20°C, DNA was quantified using a SAFIRE fluorescence plate reader. A standard curve was constructed using calf thymus DNA. Apoptotic cells were detected using a fluorescence FragEL kit QIA39 (Oncogene Research Products) according to the manufacturer's instructions. Briefly, in this assay terminal deoxynucleotidyl transferase binds to 3'-OH ends of DNA fragments in apoptotic cells and catalyzes the addition of FITC-labeled deoxynucleotides. Nonapoptotic nuclei were labeled with Hoechst 33342 dye (Molecular Probes), and preparations were examined using fluorescence microscopy (Olympus, Melville, NY). Five random $\times 40$ magnification fields per clone were recorded using Optronics MagnaFire software (Optronics, Galeta, CA). The number of nonfragmented, FITC-labeled, apoptotic nuclei (green) and Hoechst dye-stained normal nuclei (blue) was counted on coded images by two independent observers who did not know the origin of the images. Homogenates of each of the six clones were assayed using an EnzChek caspase-3 assay kit no. 2 (Molecular Probes) according to the manufacturer's instructions. For UV irradiation, confluent monolayers in 60-mm dishes were rinsed to remove all floating cells, and fresh medium was added. A short-wave UV light was placed 8 cm above the culture dish, and the cells were exposed for 3 min. After a 5-h incubation period, the floating cells were harvested and counted.

Methyl- β -Cyclodextrin Treatment

Occ⁺ and Occ⁻ monolayers were cultured on Millicell HA inserts for 6 days. Membrane cholesterol was then depleted by adding 10 mM methyl- β -cyclodextrin (MBCD) in DMEM, 1% serum to both insert and well and incubating them at 37°C (12). After 2 h, MBCD was removed; monolayers were rinsed and incubated in DMEM. TER was measured at intervals throughout the experiment.

Rhotekin Pull-Down Assay

Confluent Occ⁺ and Occ⁻ monolayers were treated with 10 mM MBCD, as described above. Rhotekin-RBD pull-down assays (Upstate Cell Signaling Solutions, Lake Placid, NY) were conducted at 0, 0.5, 1, and 2 h after the addition of MBCD according to the method of Ren et al. (32). Total RhoA and Rho-GTP were detected on Western blots using rabbit anti-Rho A antibody (Santa Cruz Biotechnology, Santa Cruz, CA), followed by horseradish peroxidase-conjugated goat anti-rabbit IgG.

Fluorescence and Confocal Laser Scanning Microscopy

Confluent monolayers of Occ⁺ and Occ⁻ cells, cultured on Nunc inserts for 5 days were fixed in 1% paraformaldehyde in DPBS and permeabilized with 0.2% Triton X-100. They were dual immunolabeled with rabbit antioccludin polyclonal antibody (pAb) and rat anti-ZO-1 monoclonal antibody, followed by Alexa 488 goat anti-rabbit IgG and Cy3 goat anti-rat pAb, respectively. Similar indirect immunofluorescent studies were conducted using pAbs to detect claudin-1, -2, -4, and -7.

MBCD-treated monolayers of Occ⁺ and Occ⁻ cells and their respective controls were labeled with rhodamine-tagged phalloidin (Molecular Probes) and examined with the use of confocal laser scanning microscope (model TCSNT, Leica, Exton, PA) (25).

Electron Microscopy

Confluent monolayers of Occ⁻ and Occ⁺ cells in 42-mm-diameter Costar polyester inserts were fixed in 2% glutaraldehyde in 0.1 M

phosphate buffer, pH 7.2, for 30 min at 4°C and dehydrated in graded alcohol. The membrane was removed from the plastic housing of the insert, cut into 2-mm-wide strips and embedded in Epon. Ultrathin sections were examined with an electron microscope (model 301, Philips).

Freeze Fracture

Confluent monolayers of Occ⁻ (clones D12 and F36) and Occ⁺ (clones G2 and G4) cells, cultured in 75-mm-diameter Costar inserts for 5, 6, or 7 days, were fixed in 2% glutaraldehyde in DPBS for 20 min at 4°C. They were rinsed in DPBS, scraped from the substrate, and infiltrated with 25% glycerol in 0.1 M cacodylate buffer, pH 7.3, for 60 min at 4°C. Cell pellets were frozen in liquid nitrogen slush and freeze fractured at -115°C in a Balzers 400 freeze-fracture unit (Balzers, Liechtenstein). After being cleaned with sodium hypochlorite, replicas were examined by electron microscopy. The width of the TJ was measured and the number of parallel and cross-bridging strands in the TJs was counted at 1-cm intervals on coded electron micrographs at a magnification of $\times 62,500$.

RESULTS

Suppression of Occludin Expression

Six clones were identified in which occludin mRNA and protein expression was suppressed by 96–98%, as determined by Northern and Western blot analysis, respectively (Fig. 1, *B* and *C*). By contrast, occludin mRNA and protein expression was clearly present in the six control clones that were transfected with a nonsuppressive occludin siRNA that did not suppress occludin expression in transiently transfected COS-7 cells. Expression levels were similar to those of the nontransfected parent cells (data not shown). The absence of occludin expression was further confirmed by dual immunolabeling of Occ⁻ and Occ⁺ monolayers for occludin and ZO-1. Negligible occludin staining was detected in the six Occ⁻ clones, whereas it was normally distributed at the TJ in the six Occ⁺ clones (Fig. 2*A*). Cells in all six Occ⁻ monolayers were somewhat more uniform in shape than those of Occ⁺ control cells, which displayed a more varied morphology.

Cell Ultrastructure and Appearance of TJs in Freeze-Fracture Replicas are Similar in Occ⁻ and Occ⁺ Clones

No discernible difference was found in transmission electron micrographs (data not shown) or in freeze-fracture replicas of Occ⁻ and Occ⁺ monolayers (Fig. 2*B*). Similarly, morphometric analysis of freeze-fracture replicas showed no statistically significant difference in the number of parallel TJ strands, the number of cross-bridging strands or the mean width of TJs in any of the 5-, 6-, or 7-day cultures.

Protein Levels of Several Members of the Claudin Family are Altered in Occ⁻ Clones

Western blots from monolayers of each of the six Occ⁻ and Occ⁺ clones, which had been cultured for 6–7 days at confluence, were probed for occludin, claudin-1, -2, -3, -4, and -7 (claudins expressed in MDCK II cells and to which antibodies were available); ZO-1, -2, and -3; E-cadherin; JAM-1; tubulin; and actin. Lysates from 3–5 independent experiments with all clones were quantified by densitometry on Western blots from gels in which equal amounts of lysate protein were loaded per lane. As indicated above, occludin expression was reduced by

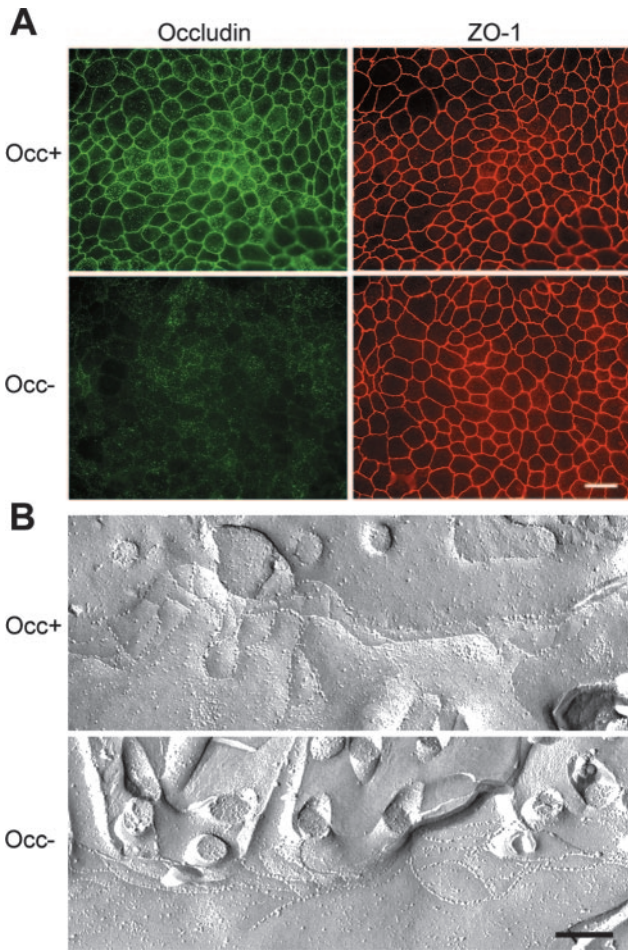


Fig. 2. *A*: representative immunofluorescent micrographs of Occ+ (clone G2) and Occ- (clone F36) monolayers. Occludin (green) and ZO-1 (red) are immunolabeled as described in MATERIALS AND METHODS. Immunolabeling for occludin is negligible in Occ- monolayers, whereas immunolabeled ZO-1 is readily detected in these monolayers. Bar represents 20 μm . *B*: representative freeze-fracture replicas of tight junctions (TJs) in Occ+ (clone G2) and Occ- (clone D12) confluent monolayers cultured for 6 days. Their ultrastructural appearance is similar. Bar represents 160 μm .

96–98%. Of the claudins examined, the amount of claudin-1 and -7 in Occ- clones was reduced by 49% and 33%, respectively, compared with Occ+ clones ($P < 0.0001$). By contrast, claudin-3 and -4 were increased by 18% ($P < 0.01$) and 63% ($P < 0.0001$), respectively, in Occ- compared with Occ+ clones, while levels of claudin-2 were unchanged. There was no change in expression levels of the three ZO proteins, E-cadherin, JAM-1, or actin. However, tubulin levels were increased by 25% ($P < 0.01$) (Fig. 3). The distribution of claudins in the cells was similar in both Occ- and Occ+ monolayers, and increased vesicular staining was not detected (data not shown).

No difference in TX-100 extractability of TJ proteins (claudin-1, -2, -3, -4, or -7) or TJ-related proteins (JAM-1, E-cadherin, ZO-1, caveolin, actin) was detected in Occ- clones compared with Occ+ clones (data not shown).

TJ Fence Function is not Impaired in Occ- Cells

Application of BODIPY-sphingomyelin to the apical surface of confluent monolayers was used to test whether occludin is

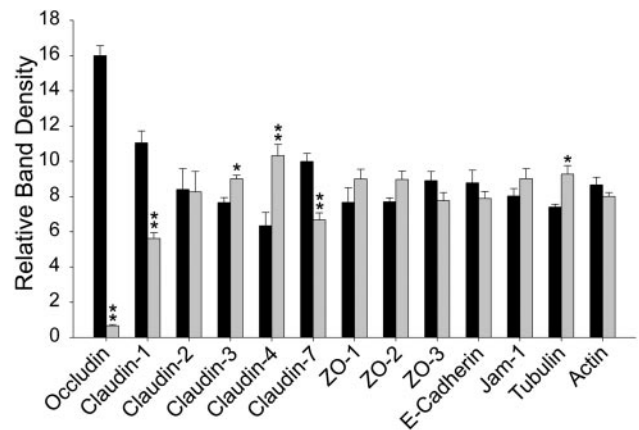


Fig. 3. Densitometric measurements of junctional protein bands on Western blots. Expression levels of occludin, claudins-1–4 and -7, ZO-1–3, junctional adhesion molecule-1 (JAM-1), E-cadherin, and actin in each of the 6 Occ+ (solid bars) and the 6 Occ- (gray bars) clones were measured by densitometry. Occ+ and Occ- samples were run on the same gel. Levels of claudin-1 and -7 expression were 49% and 33% lower in Occ- relative to Occ+ clones. By contrast, there was an 18% and 63% increase in claudin-3 and -4 expression, respectively, and a 25% increase in tubulin levels in Occ- relative to Occ+ clones. Expression of the remaining proteins was not statistically significantly different. $**P < 0.0001$ and $*P < 0.01$ by two-tailed *t*-test.

necessary to prevent the diffusion of lipids in the plane of the plasma membrane from the AP to the BL domains. Up to 1 h after application of BODIPY-sphingomyelin to the AP surface of confluent Occ- and Occ+ monolayers, the fluorescence-labeled lipid remained confined to the AP cell membrane and did not traverse the TJ (Fig. 4), indicating that occludin is not needed to maintain the “fence” function of the TJ. The possibility, however, cannot be excluded that as little as 2–4% of the cell’s occludin might be sufficient to maintain the fence function of the TJ.

Lack of Occludin Alters Peak TER Levels but not Steady-State TER

De novo TJ formation. Cells from each of the six Occ- and Occ+ clones were plated at 2 \times confluence and cultured for 3 h in calcium-sufficient medium. Nonadherent cells were removed by being rinsed with medium, and TJ formation was monitored by measuring TER at timed intervals. The time required to reach peak TER, ~ 25 h, was the same for both sets of clones; however, the maximum TER achieved by Occ- clones was between 50 and 75% lower than that of the Occ+ clones (Fig. 5A). Final steady-state TER for all 12 clones, however, was similar (Occ+ 61 ± 12 vs. Occ- $49 \pm 5 \Omega\text{cm}^2$).

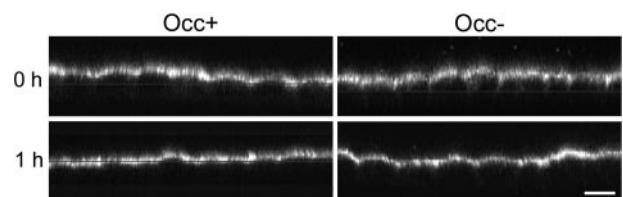


Fig. 4. Representative monolayers of Occ+ (clone G4) and Occ- (clone D12) cells were labeled with BODIPY-sphingomyelin applied to the apical surface, as described in MATERIALS AND METHODS. Images were recorded by confocal laser scanning microscopy, either immediately (0 h) or after incubation for 1 h on ice. The fluorescent dye remained confined to the apical surface of the monolayer. Bar represents 10 μm .

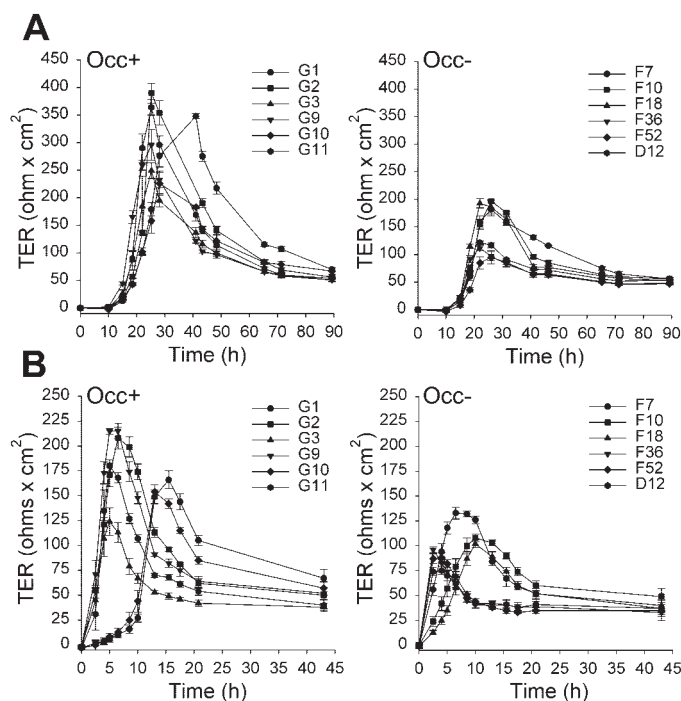


Fig. 5. *A*: de novo TJ formation in Occ+ (6 clones) and Occ- (6 clones) monolayers monitored by transepithelial electrical resistance (TER) measurements. The rate at which peak TER was attained is similar in both groups; however, peak TER values are ~50–65% lower in Occ- than in Occ+ monolayers. *B*: TJ formation in a calcium switch assay. Briefly, confluent monolayers of 6 Occ+ and 6 Occ- clones were cultured for 5 days in Ca²⁺-sufficient medium and then incubated in Ca²⁺-free medium for 24 h. TER was monitored at intervals after adding Ca²⁺-sufficient medium. In all monolayers, peak TER was attained more rapidly than during de novo TJ assembly; however, peak TER of Occ- clones was 50–65% below that of the Occ+ clones.

TJ formation in calcium switch assay. The ability to reform TJs after the addition of Ca²⁺ to monolayers previously depleted of Ca²⁺ (calcium switch assay) was also examined in the 12 clones. Cells were plated as described above and cultured for 5 days in Ca²⁺-sufficient medium. After being rinsed, monolayers were cultured in Ca²⁺-free SMEM for 24 h. The latter time period was selected to ensure that all TJs were open and that their assembly would be synchronized. The medium was then changed to Ca²⁺-sufficient medium, and TER was monitored at timed intervals. While there was a tendency in both the Occ- and Occ+ clones to segregate into two groups, with the first attaining peak TER somewhat more rapidly than the second group, the time required for Occ- clones to reach peak TER was not significantly different from that of Occ+ clones (Occ- 3–10 h vs. Occ+ 6–15 h). Except for an overlapping peak TER achieved by a single pair of monolayers (Occ+ clone G3 vs. Occ- clone F7), peak TER was ~65% lower in Occ- than in Occ+ clones, but the final average steady-state TER was similar (Occ+: 51 ± 11 vs. Occ-: 39 ± 6 Ω × cm²) (Fig. 5B).

Monolayers of Occ- Cells Exhibit Altered Paracellular Ion Permeability

The relative paracellular permeability to Na⁺ and Cl⁻ ions was monitored under current-clamp conditions by imposing a 2:1 concentration gradient of NaCl from apical to the basal side

of the monolayer, thereby inducing a potential difference, apical negative, that was similar in Occ- (-14.4 ± 0.7 mV) and Occ+ monolayers (-13.9 ± 1.4 mV), $P > 0.5$, indicating that the TJs of both Occ- and Occ+ monolayers are more permeable to Na⁺ than to Cl⁻. However, the absolute paracellular permeability to Na⁺, but not to Cl⁻, was modestly but consistently increased in Occ- monolayers, leading to an increased P_{Na-to-Cl} ratio as evidenced by the increase in dilution potential from -13.9 to -14.4 mV. Permeability to inorganic monovalent cations, including Rb⁺ and Cs⁺, was also augmented, suggesting that the structure of the pores formed by claudins in the TJs and/or the dynamic behavior of the TJ strands was altered by the absence of occludin (Fig. 6, A and B). Surprisingly, TJ permeability to a series of large monovalent organic cations, including methylamine, ethylamine, tetramethylammonium, choline, and arginine, ranging in diameter from 3.78 to 6.96 Å, was disproportionately increased (Fig. 6B). These increases in cation permeability were detected 6–7 days after plating and were less prominent in monolayers cultured for only 5 days.

Paracellular Pathway of Occ- Clones is More Permeable to Ethanamine and Mannitol but not to FITC-Dextran

The permeability of Occ- and Occ+ monolayers was also evaluated using [¹⁴C]ethanamine (an organic cation 4.9 Å in diameter), [³H]mannitol (a noncharged solute 7.2 Å in diameter) or FITC-dextran (3 and 10 kDa) flux assays. In the case of ethanamine and mannitol, the assays were conducted under two experimental conditions. In the first (BL-to-AP flux under equal hydrostatic pressure), the fluid in the insert was maintained at the same level as that in the well, and in the second (AP to BL under increased hydrostatic pressure), the fluid in the insert was 3.5 mm above that in the well, as described in MATERIALS AND METHODS. Ethanamine flux through the paracellular pathway was consistently higher in Occ- than in Occ+ monolayers, regardless of whether hydrostatic pressure was applied or not (Fig. 6C). By contrast, mannitol flux was increased in Occ- monolayers only under conditions of increased hydrostatic pressure (Fig. 6C). Flux of either 3- or 10-kDa FITC-dextran was the same in both Occ- and Occ+ clones (Fig. 6D).

Cell Density of Occ- Monolayers is not Significantly Lower than in Occ+ Monolayers

Cells in confluent monolayers of Occ- clones appeared more uniform in shape and less densely packed than Occ+ cells. To determine whether a lower rate of cell proliferation and/or a lower saturation cell density could account for these observations, DNA was quantified at timed intervals after plating the cells in 96-well plates. Whereas the amount of DNA was less in Occ- relative to Occ+ clones throughout the experiment (2.6 ± 0.2 vs. 3.1 ± 0.5 on day 1 and 4.8 ± 0.4 vs. 5.1 ± 0.2 μg/well on day 8), the difference did not reach statistical significance. We also conducted cell counts on monolayers of the six Occ- and six Occ+ clones, stained with Hoechst dye and photographed at ×40. The number of Occ- cells (4.4 × 10⁵ ± 0.38 × 10⁵ cells/cm²) was not statistically significantly different from the Occ+ cells (4.6 × 10⁵ ± 0.43 × 10⁵ cells/cm²).

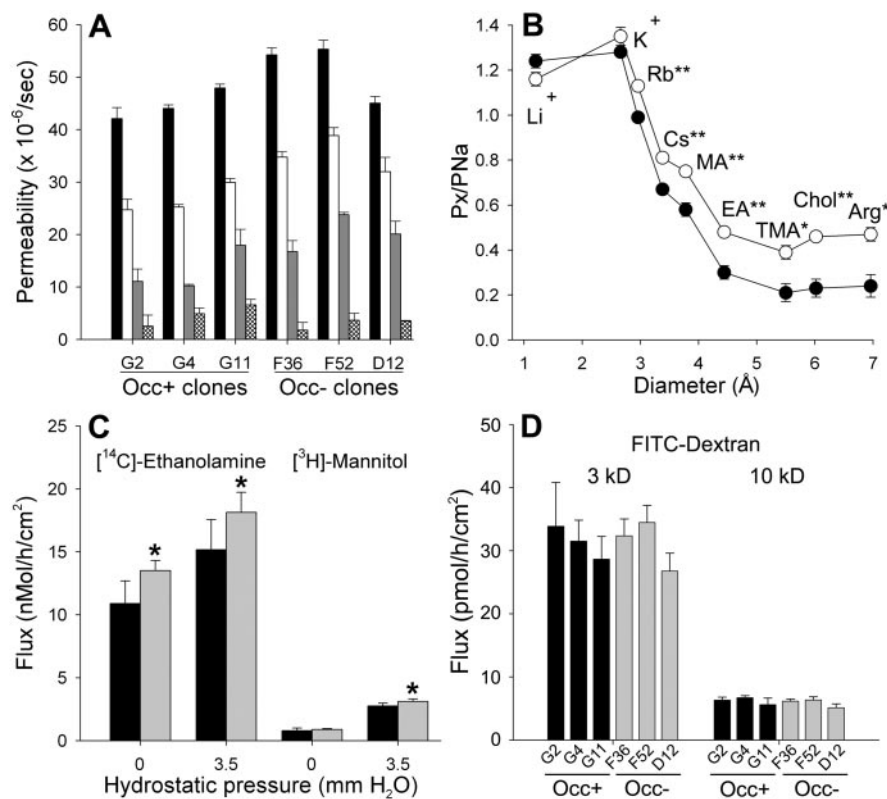


Fig. 6. Effect of occludin suppression on TJ permeability. A: permeability to individual ions was determined from dilution and bionic potential measurements of triplicate monolayers using Ussing chambers. Each bar represents the mean \pm SE of three monolayers/clone. Relative to Occ+ clones (G2, G4, G11), the mean permeability ($\times 10^{-6}$ cm/s) of Occ- clones (D12, F36, and F52) is higher for Na⁺ (solid bar) ($P > 0.005$), methylamine (open bar) ($P < 0.0001$) and arginine (gray bar) ($P < 0.0045$), but not for chloride (cross-hatched bar) ($P < 0.16$). B: effect of occludin suppression on cation size selectivity. Permeability to the indicated inorganic and organic cations, expressed as a ratio of the permeability to Na⁺ (P_x/P_{Na}), is plotted against the diameter of the ion. The increase in permeability to these cations of Occ- (F36 and F52) (\circ) and Occ+ (G2 and G11) (\bullet) clones ($n = 5$ monolayers/clone \pm SE) is significant: * $P < 0.005$, ** $P < 0.0005$ by two-tailed *t*-test. MA, methylamine; EA, ethylamine; TMA, tetramethylammonium; Chol, choline; Arg, arginine. C: ethanolamine and mannitol flux measurements on confluent monolayers cultured for 6 days. Flux measurements were conducted on quadruplicate monolayers of each of the 6 Occ+ (solid bar) and Occ- (gray bar) clones using either [¹⁴C]ethanolamine or [³H]mannitol. Assays were performed either in the absence (BL to AP) or presence of 3.5 mm of hydrostatic pressure (AP to BL), as described in MATERIALS AND METHODS. * $P < 0.05$ by two-tailed *t*-test. D: FITC-dextran flux measurements. There is no difference in the flux of 3- or 10-kDa FITC-dextran across monolayers of Occ+ (G2, G4, G11) or Occ- (D12, F36, F52) monolayers.

Cell-Substrate Adhesion is Unaffected by Lack of Occludin Expression

We noted during medium changes that the number of cells released into the medium from Occ- monolayers was strikingly less than from Occ+ monolayers. In fact, the number of cells extruded into the medium was fivefold less from the six Occ- compared with the six Occ+ clones (Fig. 7A). The difference was even more striking after 3 min of UV irradiation. Five hours later, there were 10-fold fewer cells released from Occ- compared with Occ+ monolayers (Fig. 7B); in fact, no released cells were detected in clone D12 monolayers. To determine whether the decrease in the number of cells in suspension might be the result of increased adhesion to the substratum of Occ- relative to Occ+ cells, Vybrant cell adhesion assays (Molecular Probes) were conducted. While Occ- clones F36 and D12 showed a slightly lower rate of cell substrate adherence in the first 2 h, the rate of adherence of the six Occ- and six Occ+ clones was the same by 4 h (data not shown).

Occ- Clones Retain More Apoptotic Cells in Monolayer

The observation that Occ- monolayers at steady state were composed of similar numbers of cells per unit area as Occ+ monolayers could not account for the reduction by five-fold in the number of cells extruded from confluent Occ- monolayers. To determine whether this was due to the retention of apoptotic cells in the monolayer, apoptotic nuclei were detected by staining confluent monolayers of the 12 clones using Fluorescent FragEL labeling, as described in MATERIALS AND METHODS. Two types of apoptotic nuclear structures were

labeled: 1) scattered FITC-labeled apoptotic nuclear fragments, which were found by electron microscopy to be located in and between epithelial cells (data not shown), and 2) condensed intact FITC-labeled apoptotic nuclei. Because it was not possible to determine how many fragments arose from a single nucleus, accurate counts of these fragmented nuclei were, therefore, precluded. We noted that a subset of apparently intact nuclei, $>5 \mu\text{m}$ in diameter, were FragEL labeled, and it is this subset that was counted. The data represented in (Fig. 7C), therefore, are an underestimation of the total number of apoptotic cells retained in the monolayers. Nevertheless, a threefold increase in the number of these nonfragmented apoptotic nuclei was observed in Occ- compared with Occ+ monolayers ($P < 0.012$). These observations, however, did not distinguish between an increased rate of apoptosis and an inability to extrude apoptotic cells. Utilizing EnzChek caspase-3 assays (Molecular Probes), we observed no difference in caspase-3 activity among the 12 clones (data not shown), suggesting that the increased number of cells with labeled intact apoptotic nuclei in Occ- monolayers was the result of an impaired ability to 1) sense the presence of neighboring apoptotic cells and to transmit this information to the cells' interior, or 2) extrude the apoptotic cells into the medium. Successful extrusion of cells from the monolayer involves transmitting the requisite signals from the cell surface, the activity of the actin cytoskeleton, and the reorganization of TJs to prevent a loss of TJ barrier function (23). Because extrusion of apoptotic cells in confluent monolayers is a relatively slow process involving few cells at any given time, we turned to a different strategy to test the ability of the monolayers to reorganize their actin cytoskeleton.

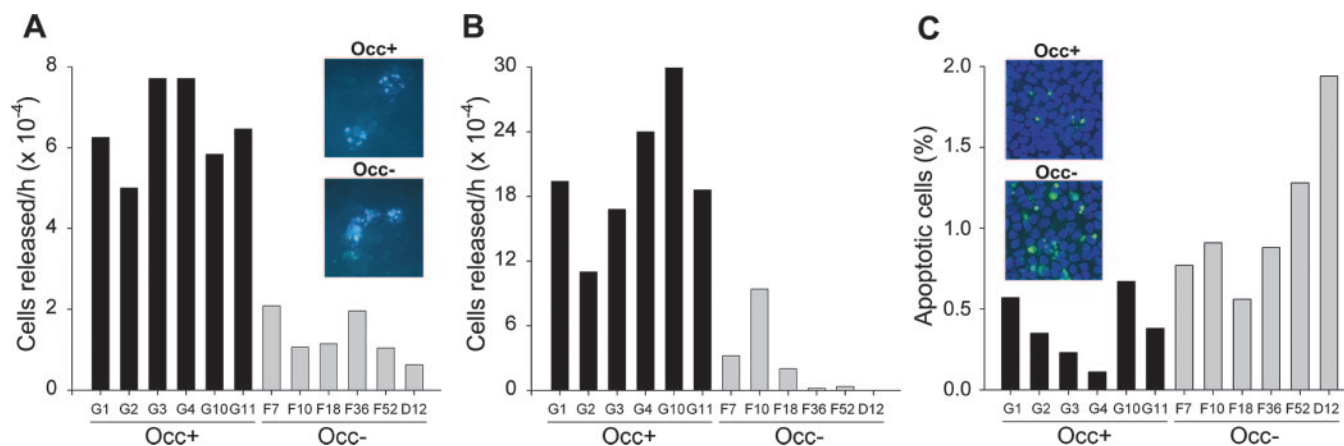


Fig. 7. A: quantification of cells extruded from the monolayer. Number of cells released per hour into the medium was calculated from 6-day confluent monolayers in 25-cm² flasks 48 h after the last medium change. There were 5 times fewer cells in supernatants of Occ⁻ (gray bars) relative to Occ⁺ clones (solid bars). *Insets*: the majority of extruded cells stained with Hoechst dye had fragmented, apoptotic nuclei. B: number of extruded apoptotic cells following UV irradiation. Monolayers of Occ⁺ and Occ⁻ monolayers cultured at confluence for 5 days were exposed to UV radiation for 3 min. Five hours later apoptotic cells released into the medium were harvested and counted. There were 10-fold fewer cells extruded from the Occ⁻ (gray bars) compared with the Occ⁺ (solid bars) monolayers. No released cells were detected in clone D12. C: number of apoptotic cells retained in monolayers. Intact nuclei were labeled with Hoechst dye, and apoptotic nuclei were detected using a fluorescein-FragEL detection kit. FragEL-labeled intact apoptotic nuclei, measuring >5 μ m in diameter, were counted in 5 random fields on coded images. FragEL-positive nuclei in each of the 6 Occ⁺ (solid bars) and 6 Occ⁻ (gray bars) clones are shown as a percentage of total Hoechst-stained nuclei. *Insets*: representative fields.

Monolayers of Occ⁻ Cells Maintain TER After Cholesterol Depletion

MBCD efficiently removes cholesterol from the plasma membrane of confluent MDCK II cell monolayers, producing an initial rapid 40% rise in TER and a fall in TER to zero by 2 h, which is accompanied by a reorganization of the subcortical actin at the cell membrane (12). In the present study, monolayers of Occ⁺ and Occ⁻ cells were treated with 10 mM MBCD for 2 h and TER was monitored at timed intervals. After the addition of MBCD, both Occ⁺ and Occ⁻ monolayers responded with an initial rise in TER; however, in contrast to Occ⁺ cells, TER did not fall to zero in Occ⁻ cells, but was maintained at or slightly below that of untreated, control monolayers; TER of Occ⁺ controls fell to near zero during this time (Fig. 8A).

RhoA-GTP is Reduced in Occ⁻ Cells

RhoA is one of several small GTP binding proteins involved in regulating the activity of the cortical actin cytoskeleton (5). It is activated by a guanylate exchange factor (GEF), one of which, GEF-H1, regulates paracellular permeability to small hydrophilic molecules (3). Activated Rho-GTP stimulates a cascade of reactions involving Rho kinase, myosin light chain, and its respective kinase and phosphatase, which result in rearrangement of the actin cytoskeleton (4) and possibly in cell signaling (34). Integral TJ proteins are linked either directly or indirectly to the actin cytoskeleton (45). Because alterations in actin distribution are coincident with the fall in TER when cholesterol is depleted (12), we measured levels of Rho-GTP in Occ⁺ and Occ⁻ monolayers after incubation for 0, 0.5, 1, and 2 h with MBCD. Using a Rhotekin pull-down assay (Upstate) (33), we determined that both Occ⁺ (G2, G4, G11) and Occ⁻ clones (D12, F36, and F52) expressed similar amounts of RhoA ($P > 0.05$), as determined using the Bonferroni multiple-comparison test. However, after MBCD treatment, Rho-GTP was significantly increased at 2 h in Occ⁺, but not in Occ⁻

cells ($P < 0.01$) (Fig. 8B), a time when TER fell rapidly in Occ⁺, but not in Occ⁻ monolayers. When monolayers were labeled with rhodamine phalloidin, an accumulation of actin formed at tricellular areas in Occ⁺ cells, but not in Occ⁻ cells, after incubation with MBCD for 2 h (Fig. 8C). This suggests that in the absence of occludin, signals produced by the rapid removal of membrane cholesterol were not transmitted from the cell membrane to intracellular RhoA.

DISCUSSION

Mounting evidence indicates that claudins, which have extracellular domains with a wide range of isoelectric points (27), form ion pores within TJ strands (42). The ion selectivity of these channels appears to be determined by charged amino acid residues in the extracellular domains of the claudins expressed in the TJs of a given tissue (8, 9, 14, 46, 47). It is important to note, however, that TJ strands themselves are not static structures. When fibroblasts are transfected with GFP-labeled claudin-1, focal aggregates of TJ strands form where two cells overlap. These structures are remarkably dynamic, with TJ strands forming end-to-end and end-to-side associations that undergo continual reorganization (40). These studies support the notion that integral TJ proteins, including occludin and claudins, are linked to and are dynamically regulated by the actin cytoskeleton (24, 41, 45). The function of occludin in the TJ, however, remains elusive.

When occludin is overexpressed in cultured epithelial cells, TER rises but mannitol flux also increases (2, 26). To explain these seemingly paradoxical results, it has been suggested that there are two routes through the TJ (1). One route, permeable to larger solutes such as mannitol and dextrans, is due to an increase in the number of dynamically regulated channels that allow the relatively slow permeation of the solute across the monolayer over time, as it diffuses from one TJ strand-bounded intercellular compartment to another. The second allows the passage of small inorganic ions when an external

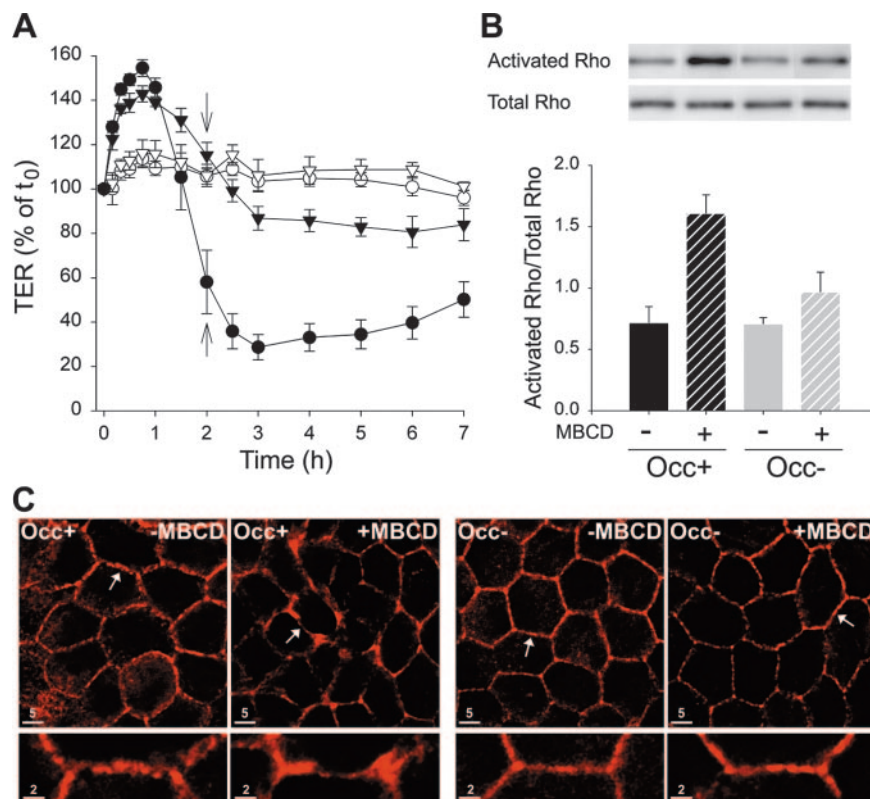


Fig. 8. *A*: cholesterol depletion. Mean TER of quadruplicate Occ+ (G2, G4, G11; circles) and Occ- (D12, F36, F52; triangles) monolayers treated with (solid symbols) or without (open symbols) 10 mM methyl- β -cyclodextrin (MBCD), as described in MATERIALS AND METHODS. MBCD was removed after 2 h (arrows), and media were changed for all monolayers. TER was measured at intervals throughout the experiment. TER in Occ- monolayers did not decline significantly and remained at a level slightly below that of untreated controls. *B*: level of activated Rho (Rho-GTP) was assessed using Rhotekin pull-down assays at the end of a 2-h incubation with 10 mM MBCD. A representative Western blot is shown. MBCD-treated Occ+ clones (G2, G4, G11), but not Occ- (D12, F36, F52) clones, expressed increased amounts of activated Rho (Rho-GTP). This difference was observed after 2 h of MBCD treatment and not at earlier time points. Density of the total RhoA bands indicates that similar amounts of total RhoA are present in both Occ+ and Occ- cells. The bar graph represents the means \pm SE of six independent experiments. *C*: representative confocal micrographs of Occ+ and Occ- cell monolayers treated with 10 mM MBCD for 2 h and labeled for actin using rhodamine-phalloidin. Just below the junctional complex, aggregates of actin are formed at cellular areas in Occ+ but not in Occ- monolayers. Small white arrows indicate the segment that is enlarged in bottom row. Bars are 5 and 2 μ m, respectively.

voltage is applied and reflects the number of current-carrying channels that are open at any given instant in time. In this model overexpression of occludin would increase the number of resistors or decrease the number of open ion pores (elevation in TER), but the channels permeable to solutes would either open for longer periods or be more numerous than in controls (increased mannitol flux).

Overexpression strategies have been useful for examining the function of selected TJ proteins in cultured cells; however, interpretation of results is complicated by the fact that the overexpressed protein may interfere with the function of the endogenous protein. To overcome this problem, we employed stable siRNA expression (6) to examine at the cellular level the effect of downregulated occludin expression on TJ function. A high degree of stable occludin suppression was achieved in Occ- clones. Furthermore, the phenotype of the Occ+ clones, transfected with a nonsuppressive occludin siRNA, was similar to that of the parent MDCK cell line. By examining six independent clones each of Occ- and Occ+ cells, effects of clonal variability were reduced.

In contrast to studies in which truncated occludin was overexpressed (2), our observations indicate that occludin does not appear to be required for the TJ's fence function. The TJs of Occ- clones, consisting almost solely of claudins, were as competent as those of Occ+ clones in preventing diffusion of BODIPY-sphingomyelin from the apical to the basolateral membrane domain. Thus claudins do not appear to require the presence of occludin to maintain a fence to the diffusion of lipids in the plane of the membrane.

The absence of occludin expression reduced the initial peak TER observed during TJ assembly in MDCK II cells, but had little effect on the final steady-state value. The mechanisms

underlying the development of this initial peak TER are not fully understood. It is possible in cells lacking occludin that there are conformational changes in the remaining TJ proteins that modulate the peak TER after their phosphorylation and/or dephosphorylation (7, 17, 28, 39, 44). In addition, members of the various polarity complexes that are key to establishing cell polarity also appear to participate in TJ assembly (41). For example, a markedly attenuated peak TER is observed when siRNA is used to suppress the expression of PALS1, a component of one of the protein complexes required for establishment of cell polarity. While the mechanisms underlying the generation of the initial peak TER in cultured epithelial cells are unidentified, our data suggest that occludin plays a significant role in this process, possibly as a structural component or as a tethering site for components of the actin cytoskeleton and polarity complexes or as a site at which signaling cascades are regulated.

The absence of occludin had little effect on steady-state TER in Occ- monolayers, which is in agreement with the observation that TER of the intestinal epithelium is unchanged in occludin-deficient mice (38). While there was an insignificant difference in TER at steady state between Occ- and Occ+ clones, there was an increase in cation but not Cl⁻ permeability. The decreased levels of claudin-1 and -7 and the increased expression of claudins-3 and -4 do not readily explain this. Claudin-4 has, in its first extracellular loop, positively charged amino acids that discriminate against the passage of monovalent, inorganic cations (9, 46). The increased expression of claudin-4 in Occ- clones should in fact decrease cation permeability. Claudin-1 and -7 are expressed not only in the TJ but also along the basolateral surface of epithelial cells (10, 16, 22, 31). Precisely how the reduced levels of claudin-1 and -7

contribute to the observed increased cation permeability is unclear. The possibility cannot be excluded that in the absence of occludin, changes in the expression of other claudins, to which there are no currently available antibodies, may also contribute to the altered cation permeability.

Interestingly, electrophysiological measurements revealed that the permeability to larger organic cations, up to 6.96 Å in diameter, was disproportionately increased relative to that of Na⁺, a finding that is consistent with the observed increased flux of [¹⁴C]ethanolamine (an organic cation 4.9 Å in diameter). This suggests the possibility that there may be two populations of cation-selective permeation pathways or pores. The first, more abundant population formed by claudins selectively facilitates the permeation of smaller inorganic cations. The ion selectivity of these pores is minimally affected by the absence of occludin. The permeability of the second less abundant population, by contrast, is dependent on the presence of occludin, which may act either directly as a structural component of this pathway or as a crucial link to the actin cytoskeleton that may regulate the opening and closing of these larger "pores." While the remarkably dynamic behavior of TJ strands composed solely of claudin-1 has recently been documented (40), similar data for TJ strands composed of a combination of claudin-1 and occludin are currently not available. It is possible that occludin might stabilize the movement of TJ strands and their interaction with the actin cytoskeleton; its absence might augment the dynamic behavior of the TJ strands. This idea is indirectly supported by the observation that overexpression of a Rho-specific guanine nucleotide exchange factor, GEF-H1, increases paracellular permeability to uncharged solutes without affecting TER (3).

The significantly smaller number of cells released into the medium in cultures of Occ⁻ clones was associated with higher numbers of apoptotic cells observed in Occ⁻ monolayers. We reasoned that this could be the result of 1) higher rates of apoptosis, 2) an inability to extrude apoptotic cells, or 3) an inability of Occ⁻ cells to sense the presence of a neighboring apoptotic cell and to transmit the appropriate signals to the actin cytoskeleton. The first possibility is excluded because we found that caspase-3 activity, a key mediator of apoptosis, was similar in both Occ⁻ and Occ⁺ cell monolayers, indicating that the larger numbers of apoptotic cells detected in the monolayers of Occ⁻ cells was not due to an accelerated rate of apoptosis. Furthermore, the reduced numbers of apoptotic cells released into the medium argued in favor of the second two possibilities. During the extrusion of apoptotic cells, maintenance of the TJ barrier is key to preserving mucosal integrity (23). This requires that neighboring cells sense the presence of an apoptotic cell in their midst and that they coordinate the activity of the actin cytoskeleton to extrude the apoptotic cell (36). To protect the integrity of the epithelial barrier, they must reorganize the TJ strands, a process that also depends on cytoskeletal activity. The fact that the TX-100 extractability of integral TJ proteins was similar in Occ⁺ and Occ⁻ clones suggests that their link to the actin cytoskeleton is intact and is not dependent on the presence of occludin.

Inhibition of RhoA, a small GTPase that regulates the activity of the actin cytoskeleton (35), impairs the ability of epithelial cells to extrude neighboring apoptotic cells (36). This suggested the possibility that in the absence of occludin, activation of RhoA might be impaired, which in turn would

impede actin cytoskeletal activity. To test whether Occ⁻ cells are able to activate RhoA, Occ⁻ cells and their Occ⁺ controls were incubated with MBCD, a strategy that elicits a rapid rise followed by a reversible fall in TER and is accompanied by a redistribution of actin (12). When MBCD was applied to confluent Occ⁻ monolayers, the initial rise in TER was observed; however, in contrast to Occ⁺ monolayers, TER did not fall significantly after a 2-h incubation with MBCD. Levels of Rho-GTP at the end of the 2-h incubation with MBCD were significantly below those of Occ⁺ monolayers. These results suggest that, in addition to being a structural component of the TJ, occludin may also function in such a way that it transmits signals originating at the plasma membrane (MBCD treatment) or in neighboring cells (apoptotic cells) to the actin cytoskeleton.

One can only speculate how the subtle changes observed in Occ⁻ MDCK cells correlate with the highly complex phenotype of occludin^{-/-} mice. The selective increase in permeability to divalent inorganic and large organic cations of TJs lacking occludin could conceivably have an impact on the barrier function of Sertoli cells, gastric epithelial cells, and brain endothelial cells, leading to testicular atrophy, inflammation of the gastric mucosa, and cerebral calcification, respectively. However, this does not explain why the TJs in other epithelia of these mice are apparently unaffected. Our observation that Rho signaling is reduced in Occ⁻ cells could also contribute to the altered phenotype of occludin^{-/-} mice because Rho participates in the regulation of TJs (29). However, further studies of the interaction of Rho and other signaling molecules with occludin directly or indirectly via cytoplasmic TJ plaque proteins are required.

ACKNOWLEDGMENTS

We gratefully acknowledge the stimulating and helpful discussions with Drs. I. Stamenkovic, S. Pilai, and A. Bernards.

GRANTS

These studies were supported by National Institutes of Health Grants HL-25822 and HL-36781 (to E. E. Schneeberger) and DK-062283 (A. S. L. Yu).

REFERENCES

1. Anderson JM, Van Itallie CM, and Fanning AS. Setting up a selective barrier at the apical junction complex. *Curr Opin Cell Biol* 16: 140–145, 2004.
2. Balda MS, Whitney JA, Flores C, Gonzalez S, Cerejido M, and Matter K. Functional dissociation of paracellular permeability from electrical resistance and disruption of the apical-basolateral intramembrane diffusion barrier by expression of a mutant membrane protein of tight junctions. *J Cell Biol* 134: 1031–1049, 1996.
3. Benais-Pont G, Punn A, Flores-Maldonado C, Eckert J, Raposa G, Fleming TP, Cerejido M, Balda MS, and Matter K. Identification of a tight junction-associated guanine nucleotide exchange factor that activates Rho and regulates paracellular permeability. *J Cell Biol* 160: 729–740, 2003.
4. Birukova AA, Smurova K, Birakov KG, Kaibuchi K, Garcia JGN, and Verin AD. Role of Rho GTPase in thrombin-induced lung vascular endothelial cells barrier dysfunction. *Microvasc Res* 67: 64–77, 2004.
5. Boivin D, Blodeau D, and Beliveau R. Regulation of cytoskeletal functions by Rho small GTP-binding proteins in normal and cancer cells. *Can J Pharmacol* 74: 801–810, 1996.
6. Brummelkamp TR, Bernards R, and Agami R. A system of stable expression of short interfering RNAs in mammalian cells. *Science* 296: 550–553, 2002.
7. Chen YH, Lu Q, Goodenough DA, and Jeanson B. Nonreceptor tyrosine kinase c-Yes interacts with occludin during tight junction formation in canine kidney epithelial cells. *Mol Biol Cell* 13: 1227–1237, 2002.

8. **Colegio OR, Van Itallie CM, McCrea HJ, Rahner C, and Anderson JM.** Claudins create charge-selective channels in the paracellular pathway between epithelial cells. *Am J Physiol Cell Physiol* 283: C142–C147, 2002.
9. **Colegio OR, Van Itallie CM, Rahner C, and Anderson JM.** Claudin extracellular domains determine paracellular charge selectivity and resistance but not tight junction fibril architecture. *Am J Physiol Cell Physiol* 284: C1346–C1354, 2003.
10. **Coyne CB, Gambling TM, Boucher RC, Carson JL, and Johnson LG.** Role of claudin interactions in airway tight junctional permeability. *Am J Physiol Lung Cell Mol Physiol* 285: L1166–L1178, 2003.
11. **Farquhar MG and Palade GE.** Junctional complexes in various epithelia. *J Cell Biol* 17: 375–412, 1963.
12. **Francis SA, Kelly JM, McCormack JM, Rogers RA, Lai J, Schneeberger EE, and Lynch RD.** Rapid reduction of MDCK cell cholesterol by methyl- β -cyclodextrin alters steady state transepithelial electrical resistance. *Eur J Cell Biol* 78: 473–484, 1999.
13. **Furuse M, Fujita K, Fujimoto K, and Tsukita S.** Claudin 1 and 2: Novel integral membrane proteins localizing at tight junctions with no sequence similarity to occludin. *J Cell Biol* 141: 1539–1550, 1998.
14. **Furuse M, Furuse K, Sasaki H, and Tsukita S.** Conversion of *zonulae occludentes* from tight to leaky strand type by introducing claudin-2 into Madin-Darby canine kidney I cells. *J Cell Biol* 153: 263–272, 2001.
15. **Furuse M, Hirase T, Itoh M, Nagafuchi A, Yonemura S, Tsukita S, and Tsukita S.** Occludin: A novel integral membrane protein localizing at tight junctions. *J Cell Biol* 123: 1777–1788, 1993.
16. **Gregory M, Dufresne J, Hermo L, and Cyr DG.** Claudin-1 is not restricted to tight junctions in the rat epididymis. *Endocrinology* 142: 854–863, 2001.
17. **Hirase T, Kawashima S, Wong EYM, Ueyama T, Rikitake Y, Tsukita S, Yokoyama M, and Staddon JM.** Regulation of tight junction permeability and occludin phosphorylation by RhoA-p16OROCK-dependent and -independent mechanisms. *J Biol Chem* 276: 10423–10431, 2001.
18. **Hynes RO and Wagner DD.** Genetic manipulation of vascular adhesion molecules in mice. *J Clin Invest* 98: 2193–2195, 1996.
19. **Janakidevi K, Murray CD, Sell C, and Held P.** Fluorometric analysis of DNA in cell cultures. *Anal Biochem* 172: 78–81, 1988.
20. **Laemmli UK.** Cleavage of structural proteins during the assembly of the head of bacteriophage T4. *Nature* 227: 680–685, 1970.
21. **Li D and Mrsny RJ.** Oncogenic Raf-1 disrupts epithelial tight junctions via downregulation of occludin. *J Cell Biol* 148: 791–800, 2000.
22. **Li WY, Huey CL, and Yu ASL.** Expression of claudin-7 and -8 along the mouse nephron. *Am J Physiol Renal Physiol* 286: F1063–F1071, 2004.
23. **Madara JL.** Maintenance of the macromolecular barrier of cell extrusion sites in intestinal epithelium: physiological rearrangement of tight junctions. *J Membr Biol* 116: 177–184, 1990.
24. **Matter K and Balda MS.** Signalling to and from tight junctions. *Nature Mol Cell Biol* 4: 225–236, 2003.
25. **McCarthy KM, Francis SA, McCormack JM, Lai J, Rogers RA, Skare IB, Lynch RD, and Schneeberger EE.** Inducible expression of claudin-1-myc but not occludin-VSVG results in aberrant tight junction strand formation in MDCK cells. *J Cell Sci* 113: 3387–3398, 2000.
26. **McCarthy KM, Skare IB, Stankewich MC, Furuse M, Tsukita S, Rogers RA, Lynch RD, and Schneeberger EE.** Occludin is a functional component of the tight junction. *J Cell Sci* 109: 2287–2298, 1996.
27. **Mitic LL and Van Itallie CM.** Occludin and claudins: transmembrane proteins of the tight junction. In: *Tight Junctions* (2nd ed.), edited by Cerejido M and Anderson JM. Boca Raton, FL: CRC, 2001, p. 213–230.
28. **Nunbhakdi-Craig V, Machleidt T, Ogris E, Bellotto D, White CL, and Sontag E.** Protein phosphatase 2A associates with and regulates atypical PKC and the epithelial tight junction complex. *J Cell Biol* 158: 967–978, 2002.
29. **Nusrat A, Giry M, Turner JR, Colgan SP, Parkos CA, Carnes D, Lemichez E, Boquet P, and Madara JL.** Rho protein regulates tight junctions and perijunctional actin organization in polarized epithelia. *Proc Natl Acad Sci USA* 92: 10629–10633, 1995.
30. **Powell DW.** Barrier function of epithelia. *Am J Physiol Gastrointest Liver Physiol* 241: G275–G288, 1981.
31. **Rahner C, Mitic LL, and Anderson JM.** Heterogeneity in expression and subcellular localization of claudins 2, 3, 4 and 5 in the rat liver, pancreas and gut. *Gastroenterology* 120: 411–422, 2001.
32. **Ren XD, Kiosses WB, and Schwartz MA.** Regulation of the small GTP-binding protein Rho by cell adhesion and the cytoskeleton. *EMBO J* 18: 578–585, 1999.
33. **Ren XD and Schwartz MA.** Determination of GTP loading on Rho. *Methods Enzymol* 325: 264–272, 2000.
34. **Ridley AJ and Hall A.** Signal transduction pathways regulating Rho-mediated stress fibre formation: requirement of a tyrosine kinase. *EMBO J* 13: 2600–2610, 1994.
35. **Ridley AJ and Hall A.** The small GTP-binding protein Rho regulates the assembly of focal adhesions and actin stress fibers in response to growth factors. *Cell* 70: 389–399, 1992.
36. **Rosenblatt J, Raff MC, and Cramer LP.** An epithelial cell destined for apoptosis signals its neighbors to extrude it by an actin- and myosin-dependent mechanism. *Curr Biol* 11: 1847–1857, 2001.
37. **Saitou M, Fujimoto K, Doi Y, Itoh M, Fujimoto T, Furuse M, Takano H, Noda T, and Tsukita S.** Occludin-deficient embryonic stem cells can differentiate into polarized epithelial cells bearing tight junctions. *J Cell Biol* 141: 397–408, 1998.
38. **Saitou M, Furuse M, Sasaki H, Schulzke JK, Fromm M, Takano H, Noda T, and Tsukita S.** Complex phenotype of mice lacking occludin, a component of tight junction strands. *Mol Biol Cell* 11: 4131–4142, 2000.
39. **Sakakibara A, Furuse M, Saitou M, Ando-Akatsuka Y, and Tsukita Y.** Possible involvement of phosphorylation of occludin in tight junction formation. *J Cell Biol* 137: 1393–1401, 1997.
40. **Sasaki H, Matsui C, Furuse K, Mimori-Kiyosue Y, Furuse M, and Tsukita S.** Dynamic behavior of paired claudin strands within apposing plasma membranes. *Proc Natl Acad Sci USA* 100: 3971–3976, 2003.
41. **Schneeberger EE and Lynch RD.** The tight junction: a multifunctional complex. *Am J Physiol Cell Physiol* 286: C1213–C1228, 2004.
42. **Tang VW and Goodenough DA.** Paracellular ion channel at the tight junction. *Biophys J* 84: 1660–1673, 2003.
43. **Towbin H, Staehelin T, and Gordon J.** Electrophoretic transfer of proteins from polyacrylamide gels to nitrocellulose sheets: procedure and some applications. *Proc Natl Acad Sci USA* 76: 4350–4354, 1979.
44. **Tsukamoto T and Nigam SK.** Role of tyrosine phosphorylation in the reassembly of occludin and other tight junction proteins. *Am J Physiol Renal Physiol* 276: F737–F750, 1999.
45. **Tsukita S, Furuse M, and Itoh M.** Multifunctional strands in tight junctions. *Nature Rev Mol Cell Biol* 2: 285–293, 2001.
46. **Van Itallie C, Rahner C, and Anderson JM.** Regulated expression of claudin-4 decreases paracellular conductance through a selective decrease in sodium permeability. *J Clin Invest* 107: 1319–1327, 2001.
47. **Yu ASL, Enck AH, Lencer WI, and Schneeberger EE.** Claudin-8 expression in Madin-Darby canine kidney cells augments the paracellular barrier to cation permeation. *J Biol Chem* 278: 17350–17359, 2003.